Petrogenesis of picritic mare magmas: Constraints on the extent of early lunar differentiation

John Longhi [*]

Lamont-Doherty Earth Observatory, Palisades, NY 10964, USA

Received 12 April 2006; accepted in revised form 20 September 2006

Abstract

Calculations of isobaric batch, polybaric batch, and polybaric fractional melting have been carried out on a variety of proposed lunar and terrestrial source region compositions. Results show that magmas with a generally tholeiitic character—plagioclase and high-Ca pyroxene crystallize before low-Ca pyroxene reflecting relatively high Al_2O_3 concentrations (>12 wt%)—are the inevitable consequence of anhydrous partial melting of source regions composed primarily of olivine and two pyroxenes with an aluminous phase on the solidus. Low-Al_2O_3 magmas (<10 wt%), as typified by the green picritic glasses in the lunar maria require deep (700–1000 km), low-Al_2O_3 source regions without an aluminous phase. The difference between primitive and depleted mantle beneath mid-ocean ridges amounts to less than 0.1 wt% Al_2O_3, whereas formation of the green glass source region requires a net loss of between 1.5 and 2.5 wt% Al_2O_3. Basalt extraction cannot account for fractionations of this magnitude. Accumulation of olivine and pyroxene at the base of a crystallizing magma ocean is, however, an effective method for producing the necessary Al_2O_3 depletions. Both olivine-rich and pyroxene-rich source regions can produce the picritic magmas, but mixing calculations show that both types of source region are likely to be hybrids consisting of an early- to intermediate-stage cumulate (olivine plus enstatite) and a later stage cumulate assemblage. Mass balance calculations show that refractory element-enriched bulk Moon compositions contain too much Al_2O_3 to allow for the deep low-Al_2O_3 source regions even after extraction of an Al_2O_3-rich (26–30 wt%) crust between 50 and 70 km thick.

© 2006 Elsevier Inc. All rights reserved.

1. Introduction

Ever since petrographic studies revealed anorthositic lithologies in Apollo 11 soils (Wood et al., 1970), researchers have appealed to buoyant segregation of relatively low-density plagioclase in an extensive, primordial melting event to explain the plagioclase-rich crust of the Moon. However, the notion of a complimentary, plagioclase-depleted lunar interior did not gain wide acceptance until after studies of the Apollo 12 mare basalts. Initially, the nearly ubiquitous negative Eu-anomalies in rare earth element (REE) plots of mare basalt analyses were widely interpreted as indicating residual plagioclase in the basalt source region. Eventually, experimental work by Green et al. (1971a,b) demonstrated that plagioclase was absent from the liquidus of primitive mare basalts at both low and high pressure. The inability of plagioclase to crystallize in the early stages of low-pressure differentiation or to remain a residual phase in the mare basalt source region meant that the widespread signal of plagioclase fractionation in mare basalts was actually an indication that an earlier event depleted the mare basalt source region in plagioclase (Philpotts et al., 1972). This earlier global differentiation event became the subject of numerous geochemical and geophysical models (e.g., Solomon and Töksoz, 1973; Taylor and Jakés, 1974) and eventually became known as the lunar magma ocean (Wood, 1975).

There have been numerous attempts to demonstrate the former existence of a lunar magma ocean, gauge its size, and predict its effects. Warren (1985) provides a thorough review and analysis of the problem. Although researchers have employed a variety of methods from extinct radioisotopes to seismology to constrain the evolution of the lunar

---
[*] Fax: +1 845 365 8155.
E-mail address: longhi@ldeo.columbia.edu

magma ocean, in this work I will focus on major element constraints on the composition and extent of the mare basalt source region as a means of inferring the extent of early lunar differentiation.

2. The depth and composition of the mare basalt source region

The compositions of basalts reflect the composition and depth of their source regions, although not as directly as we would like. Not only do magma compositions change prior to eruption in response to low-pressure crystallization and assimilation, but also the melting process intrinsically obscures itself. Melting in the Earth's mantle occurs primarily by the release of pressure during convective upwelling. Adiabatic decompression permits ~10% melting per GPa (Hess, 1992). Low porosity and density differences between melt and matrix lead to separation of melt from matrix during the melting process (McKenzie, 1984). Consequently, most primitive magmas are blends of low degree melts accumulated over a range of depths from a progressively depleting source. An important corollary is that a magma composition cannot be related to a specific depth by major elements. Nonetheless, there have been several reasonably

successful calculations of primitive magma composition based upon parameterization of the *P*–*T*–*X* data obtained from melting experiments (Klein and Langmuir, 1987; Kinzler and Grove, 1992a; Longhi, 1992, 2002; Hirschmann et al., 1998). The present investigation is an update of my earlier work (Longhi, 1992) that includes new parameterizations of melting equilibria based not only on a much more extensive database, e.g., Longhi (2003), but also on a new high-temperature pressure calibration (Longhi, 2005) that is discussed further in Appendix A.

2.1. Basalt compositions

In order to understand the implications of mare basalt compositions for lunar structure, it is useful to compare them to terrestrial basalts in the same format that the melting calculations are presented. Accordingly, Fig. 1 compares the compositions of low-Ti mare basalts and picritic green glasses with those of the most abundant terrestrial basalts: mid-ocean ridge (MORB), ocean island (OIB), and continental flood (CFB). Each set of compositions is projected twice: first from the wollastonite (Wo) component (Fig. 1a and c) and second from the Ol component (Fig. 1b and d). The Wo projection displays the
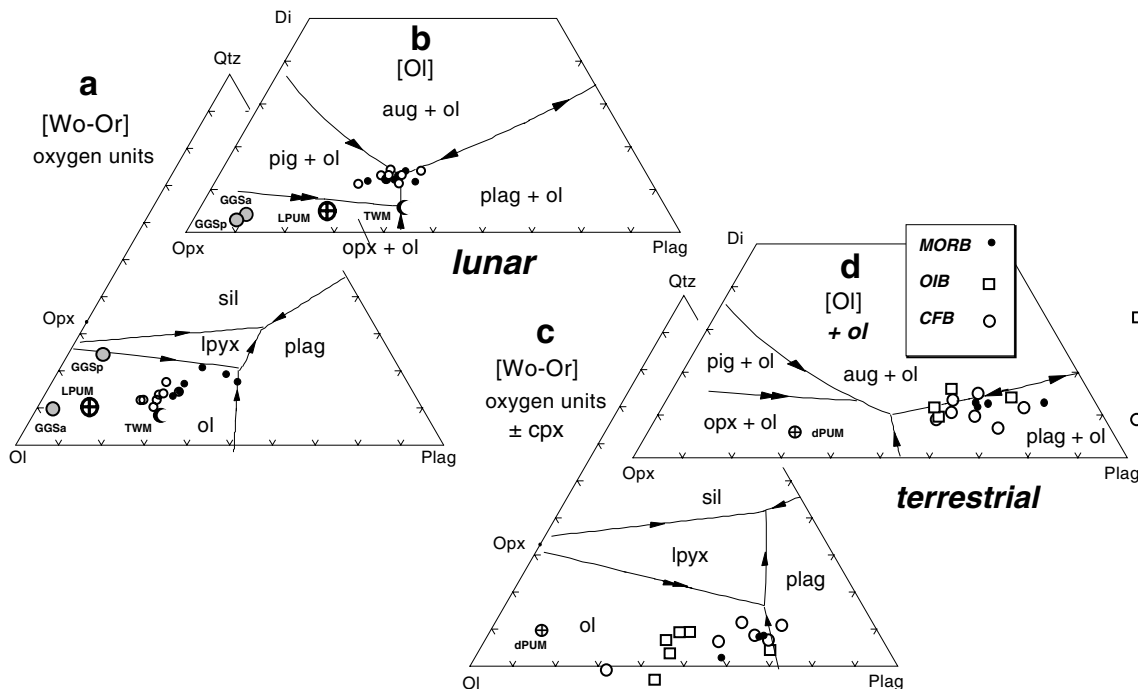

Fig. 1. Comparison of mare basalts and picritic glasses with terrestrial basalts. Each type of composition is projected in two ways: from the wollastonite (Wo) component onto the quartz (Qtz)–olivine (Ol)–plagioclase (Plag) plane (a and c), and from the olivine (Ol) component onto the lower half of the orthopyroxene (Opx)–Plag–Wo plane (b and d—Longhi, 1991). Low-pressure liquidus boundaries are calculated from the algorithms of Longhi (1991). Phase abbreviations: sil, silica; pig, pigeonite; opx, orthopyroxene; aug, augite; lpyx, low-Ca pyroxene (opx or pig); plag, plagoclase; and ol, olivine. Arrows indicate direction of decreasing temperature. (a and b) Lunar green glasses (Ap15 A, Ap16, Ap14 VLT, Ap14, Ap17 Delano, 1986) are open circles and mare basalts (15016, 15499, 12008, 12009, 14053, Luna 16 B1, Luna 24182 from Basaltic Volcanism Study Project, 1981) are solid circles; whole moon compositions are lunar primitive upper mantle (LPUM—Longhi, 2003) and Taylor whole Moon (TWM—Taylor, 1982); GGSa is green glass source composition (this study); phase boundaries drawn for Mg′ = 0.50, XAn^{liq} = 0.10, XOr^{liq} = 0.01. (c and d). Terrestrial basalts: average mid-ocean ridge basalt (MORB) glasses from Melson et al. (1976), continental flood basalts (CFB) and ocean island basalts (OIB) from Basaltic Volcanism Study Project (1981); depleted primitive upper mantle (dPUM) is from Kinzler and Grove (1992b); phase boundaries drawn for Mg′ = 0.60, XAn^{liq} = 0.50, XOr^{liq} = 0.05. Mg′ is molar MgO/(MgO + FeO); XAn^{liq} and XOr^{liq} are the mole fractions of the anorthite and orthoclase components in the liquid normative feldspar.

proportions of olivine (Ol), plagioclase (Plag), and silica (Qtz) components in basaltic liquids with Wo component $\leqslant$ that needed to saturate liquids with high-Ca pyroxene. The Ol projection displays the proportions of orthopyroxene (Opx), Plag, and Wo components of olivine-saturated liquids. In all of the diagrams low-pressure liquidus boundaries appropriate to the Mg′ value (MgO/(MgO + FeO) – molar) and normative feldspar composition of the various basalts were calculated by the algorithms presented by Longhi (1991).

The terrestrial basalts (Fig. 1c and d) have higher proportions of plagioclase (Plag) to pyroxene (Opx, Di) components reflecting higher concentrations of both Al_2O_3 and alkalis. The high relative proportions of the Plag component lead to early crystallization of plagioclase and augite and the relatively late appearance of low-Ca pyroxene as pigeonite. This is the typical crystallization pattern of tholeiites. The lower proportion of the Plag component in the low-Ti mare basalts (Fig. 1a and b) leads to the early appearance of pigeonite, usually before plagioclase. The differences in Al_2O_3, reflected in the proportions of the Plag component, are likely to reflect different magmatic histories of the respective source regions. Whereas, different abundance levels of moderately volatile alkalis in lunar and terrestrial basalts reflect different planetary accretion histories. Fig. 1a also shows that low-Ti picritic green glasses have higher propor-

tions of olivine component than do the basalts. Fig. 1b shows that once the olivine component is removed from the glasses and the basalts by projection, the glasses have pretty much the same range of composition as the low-Ti mare basalts. Thus, it is reasonable to assume that the mare basalts represent differentiates of more picritic magmas, and, therefore, the low-Ti mare basalts and green glasses probably are derived from similar source regions

2.2. Melting of the terrestrial mantle

Fig. 2 shows a series of batch and polybaric fractional melts of a source with the composition of depleted primitive upper mantle (dPUM) from Kinzler and Grove (1992b). Despite a small amount of fractionation by basalt extraction, dPUM retains approximately chondritic proportions and concentrations of refractory elements, exclusive of metal. Melt compositions were calculated with the programs, BATCH and FFTHERM (Longhi, 2002). BATCH is a high-pressure version of MAGPOX (Longhi, 1991, 1992), which calculates equilibrium partial melting. FFTHERM is a modification of BATCH that balances the amount of melting during decompression of an input source composition against the temperature drop along an adiabat of 15 °C/GPa, the calculated temperature drop along the solidus, and the temperature equivalent of the
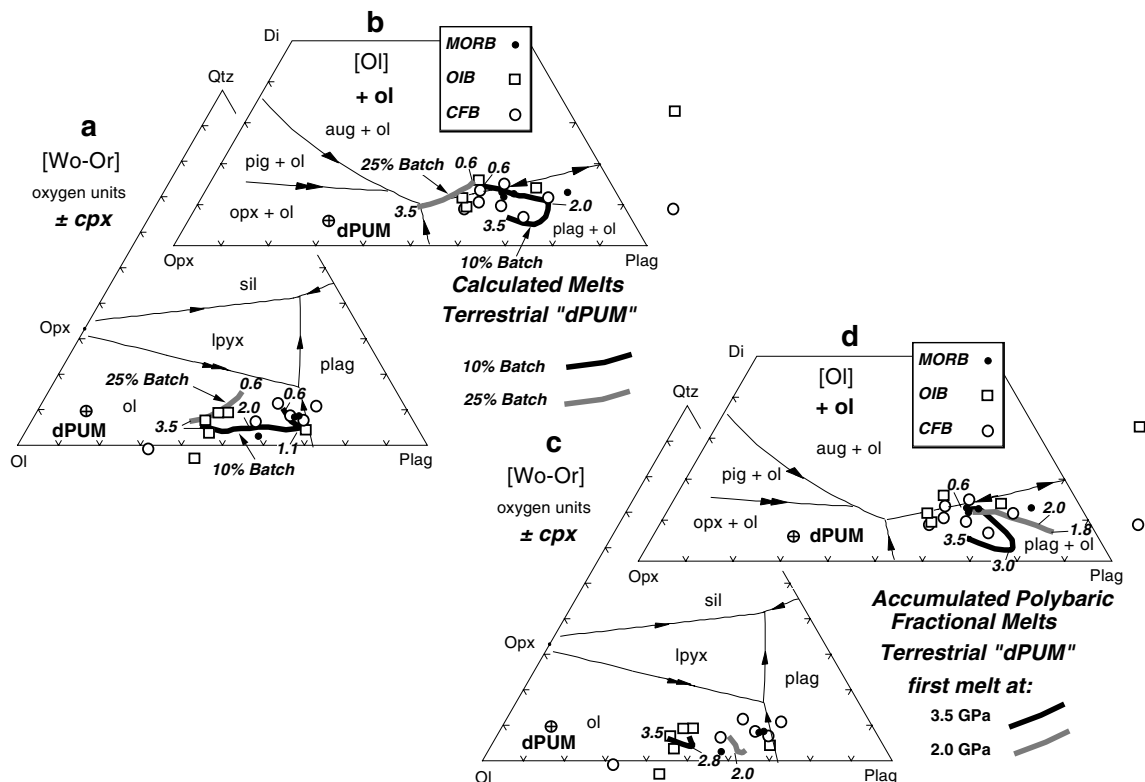

Fig. 2. Compositions of batch and accumulated polybaric fractional melts of model terrestrial upper mantle (dPUM—Kinzler and Grove (1992b). Projections and low-pressure phase boundaries are from Fig. 1. Batch melts (a and b) are 25% and 10% of dPUM at 0.1 GPa intervals from 3.5 to 0.6 GPa. Two sets of accumulated polybaric fractional melts are plotted in c and d. One begins at 3.5 GPa, the other at 2.0 GPa. Both proceed in 0.1 GPa steps and end at 0.6 GPa. Melt in excess of an assumed porosity of 0.008 is removed from source and added to the accumulating pool. Melting rate is controlled by balancing the decrease in temperature along the solidus by the adiabatic gradient (15 °C/GPa) and the temperature equivalent of the heat of fusion of peridotite (160 cal/g ÷ 0.3 cal/°C = 530 °C/g, Hess, 1992).

heat of fusion. Any portion of melt that exceeds an assumed background porosity fraction is withdrawn and accumulated. Salters et al. (2002) found that a porosity fraction of 0.008 satisfied the constraints of mantle upwelling rates and U/Th disequilibrium beneath mid-ocean spreading centers, so that value is employed here. Longhi (2002) provides an extensive analysis of the pressure and compositional dependence of the liquidus equilibria that control melting of peridotite sources.

In Fig. 2a and b the compositions of batch melts of 10% and 25% are shown for the range of 0.6–3.5 GPa. The 10% batch melts have high proportions of the Plag component and overlap the range of tholeiitic basalts. Not surprisingly the 25% batch melts have lower proportions of the Plag component than do the 10% melts at the same pressure. Nonetheless, the 25% batch melts retain a generally tholeiitic character. The 10% batch melts all represent liquids that are saturated with a highly aluminous phase (plagioclase, spinel, or garnet). Lower degrees of melting of dPUM, or similar degrees of melting of a source with higher concentrations of alkalis, or melting in the presence of CO_2 would produce liquids that project even farther to the right in Fig. 2b, and with lower, possibly negative, Qtz coordinate in Fig. 2a (cf. Longhi, 2002, for greater detail). Two of the natural basalt compositions project outside both the limits of the diagrams and the limits of the calculated melts. These compositions contain normative nepheline and probably reflect the influence of CO_2 in the melting process. The degree of melting required to exhaust the highly aluminous phase varies with pressure, but is typically in the range of 15–20%—so the compositions of dPUM melts at the point of exhaustion of the aluminous

phase during melting should lie approximately half way between the loci of 10% and 25% melts and have the general character of olivine tholeiites.

Two sequences of accumulated fractional melts (FFTHERM) are also shown (Fig. 2c and d): one beginning at 3.5 GPa; the other beginning at 2.0 GPa. As expected, the sequence of accumulated fractional melts that begins at the higher pressure produces the terminal accumulated melt (0.6 GPa) with the higher Ol and lower Plag component. Also the overall proportions of the pyroxene and plagioclase components in the accumulated melts exclusive of olivine remain consistent with the tholeiitic character of the basalts even though the accumulated melts—being comprised of a blend of ~1% melts—are quite different than the batch melts.

Taken together, the diagrams in Fig. 2 demonstrate that the presence of a highly aluminous phase in an anhydrous, peridotitic mantle, similar to that of the Earth, ensures that moderate degrees of melting of the mantle, whether single stage or accumulated, isobaric or polybaric, will produce tholeiitic magmas with high ratios of plagioclase to pyroxene components.

2.3. Melting of primitive lunar compositions

TWM, the whole Moon composition of Taylor (1982), is enriched in refractory elements relative to estimates of the Earth's composition. For example, TWM contains 6 wt% Al_2O_3 which is about 1.5 times the estimated concentration of the Earth's upper mantle (Hart and Zindler, 1986). Ten percent batch melts of TWM, shown in Fig. 3a and b, have relatively high ratios of plagioclase to pyroxene
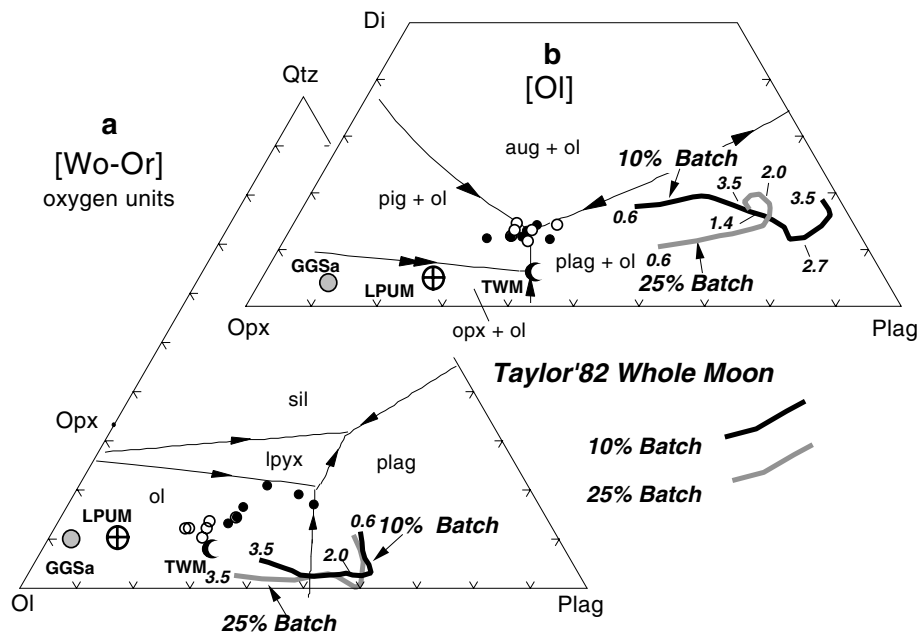

Fig. 3. Batch melts of TWM composition. Projections, low-pressure phase boundaries, and symbols from Fig. 1a and b. Ten percent and 25% batch melts of TWM (Taylor, 1982) calculated for pressures from 3.5 to 0.6 GPa in 0.1 GPa steps. All melts coexist with olivine and orthopyroxene; all 10% melts coexist with clinopyroxene; 10% melts coexist with garnet from 4.0 to 2.6 GPa, with spinel from 2.5 to 2.3 GPa, and with plagioclase from 1.4 to 0.5 GPa. Twenty-five percent melts coexist with garnet from 4.0 to 2.6 GPa. Twenty-five percent melts also coexist with clinopyroxene from 2.5 to 2.3 GPa.

components, a generally tholeiitic aspect, and do not overlap the compositions of the mare volcanic glasses (open circles) and basalts (solid circles). LPUM, a composition obtained simply by lowering the concentrations of the alkalis in the terrestrial PUM composition of Hart and Zindler (1986) to lunar levels (Longhi, 2003), contains lower Al_2O_3 than the TWM composition, but still has sufficient Al_2O_3 to stabilize highly aluminous phases at the solidus. Its batch melts (Fig. 4a and b) are generally tholeiitic and similar to the terrestrial batch melts shown in Fig. 2a and b. At 3.0–3.5 GPa the 25% batch melts of LPUM begin to approach the component proportions of the mare volcanics, because the garnet is melted out. However, Mg' values of the LPUM melts are much higher than those of the green glasses (0.80 versus 0.61), and there is no plausible way for generating ⩾25% melting at depths within the Moon corresponding to this pressure range (3.0–3.5 GPa). For example, Hess (1992) estimated a melting rate of 10%/GPa. Twenty-five percent decompression melting thus requires 2.5 GPa of decompression. However, when this 2.5 GPa is added to the pressure of interest (3.0 GPa), the result is 5.5 GPa, which is greater than the pressure at the center of the Moon (4.7 GPa).

Fig. 5 illustrates the range of accumulated polybaric fractional melts produced by the TWM and LPUM compositions for melting sequences that begin at 3.5 and 4.0 GPa, respectively. The lower Mg' of TWM causes its melts to project with lower Qtz component in the [Wo–Or] projection and lower Opx component in the [Ol] projection than melts of LPUM for similar source mineralogy and pressure. However, the solidus assemblages are not the same in the garnet stability field. Where garnet is stable, olivine, orthopyroxene, clinopyroxene, and garnet coexist on the solidus of LPUM, but orthopyroxene is absent on the solidus of TWM. The reason is interplay between bulk

composition and a peritectic involving orthopyroxene (opx + liq = ol + cpx + gar). This matter is described in some detail in Longhi (2002), but for present purposes the absence of orthopyroxene allows the composition of near-solidus melts to access low SiO_2 contents. As a result, none of the accumulated melts of TWM even remotely approach the range of low-Ti mare basalts and picritic glasses. The example of terrestrial fractional melting (Fig. 2c and d) demonstrates that beginning melting at a lower pressure will not produce mare-like magmas either. The first few melting steps of the LPUM sequence produce accumulated melts with coordinates similar to those of the green glasses in the [Wo–Or] projection. However, in the [Ol] projection these accumulated melts have much higher Wo coordinates than do the mare volcanics, reflecting the presence of residual clinopyroxene, orthopyroxene, and garnet in the source.

2.4. Melting of the green glass source (GGS) region

2.4.1. Olivine-rich compositions

The analysis so far has demonstrated that the mare volcanics were not produced by melting of primitive source regions (chondritic proportions of refractory elements). There are two very different estimates of the major element composition of the low-Ti mare basalt source region. One (TLM = Taylor lunar mantle) is the TWM composition minus the weight fraction of the lunar crust (Taylor, 1982). The TLM has more than 4 wt% Al_2O_3, which is comparable to the LPUM composition. Therefore, a homogeneous TLM mantle would produce tholeiitic melts with compositions between those of TWM and LPUM. A differentiated TLM could easily have layers similar to the GGS compositions. However, layers with low (<4 wt%) Al_2O_3 contents would necessarily be balanced
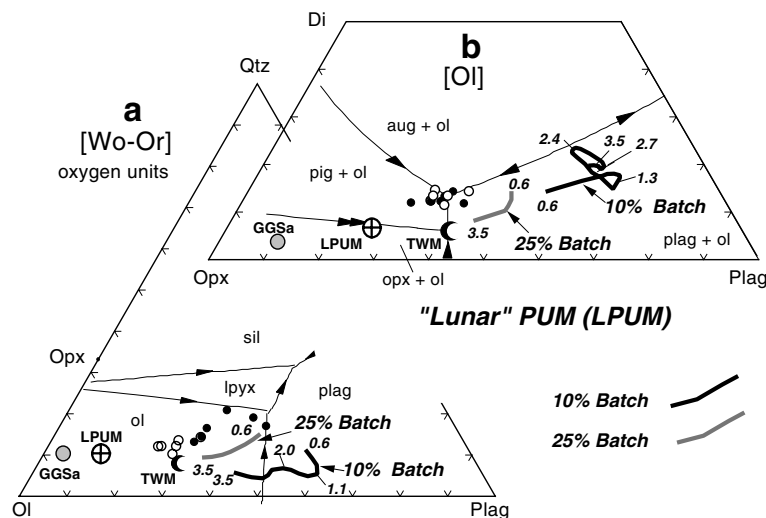
Fig. 4. Batch melts of LPUM composition. Projections, low-pressure phase boundaries, and symbols from Fig. 1a and b. Ten percent and 25% batch melts of LPUM (Longhi, 2003) calculated for pressures from 3.5 to 0.6 GPa in 0.1 GPa steps. All melts coexist with olivine and orthopyroxene; all 10% melts coexist with clinopyroxene. Ten percent melts coexist with garnet from 3.5 to 2.6 GPa, with spinel from 2.5 to 2.3 GPa, and with plagioclase from 1.4 to 0.5 GPa. Twenty-five percent melts coexist with garnet from 4.0 to 2.6 GPa.
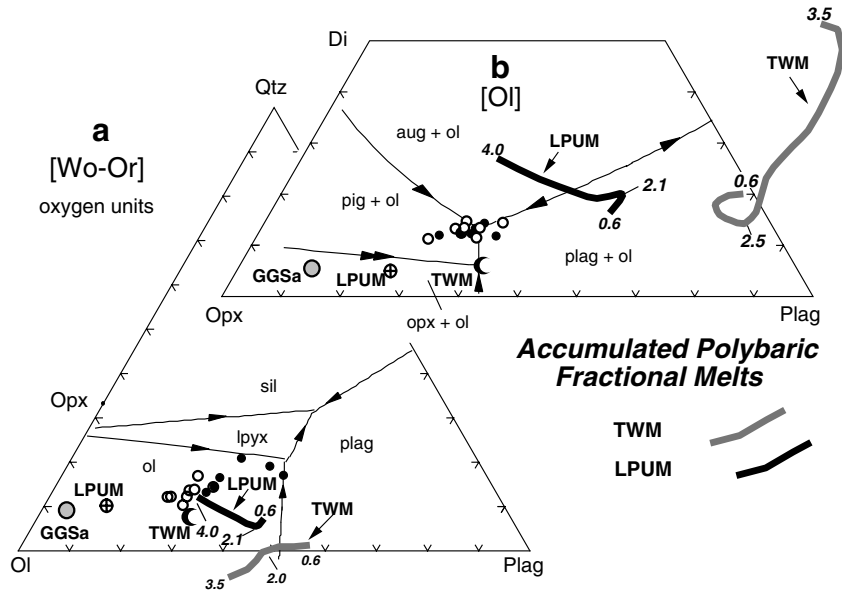
Fig. 5. Accumulated polybaric fractional melts of TWM and LPUM. Projections, low-pressure phase boundaries, and symbols from Fig. 1a and b. TWM melting path begins at 3.5 GPa. LPUM melting path begins at 4.0 GPa. Both paths end at 0.5 GPa. Melting parameters as in Fig. 2.

by complimentary layers with high (>4 wt%) Al_2O_3. This matter will be discussed below.

Longhi (1992) derived the second estimate, GGS, empirically by varying the source composition until the terminal accumulated melts had compositions similar to the green glasses. Fig. 6 illustrates three tracks of accumulated polybaric fractional melts of GGSa (Table 1), a revised version of the original GGS. Each track begins melting at a
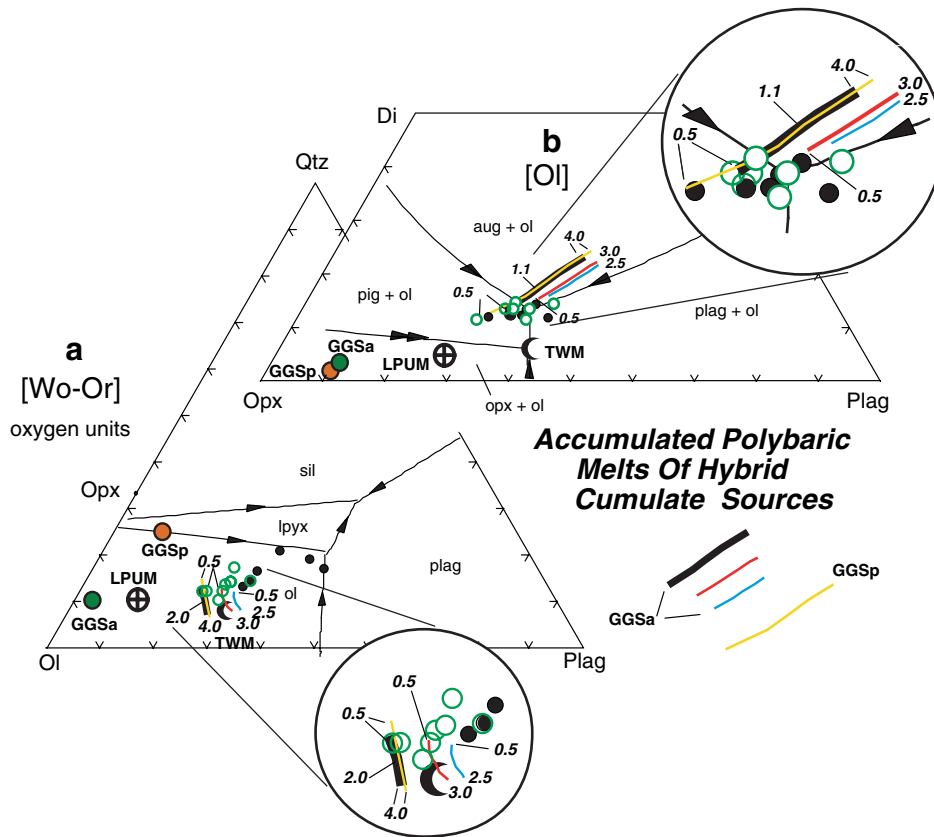
Fig. 6. Accumulated polybaric fractional melts of green glass sources, GGSa and GGSp. Projections and low-pressure phase boundaries from Fig. 1a and b. Green glasses and mare basalts are open (green) and solid (black) circles, respectively. Melting paths begin at 4.0, 3.0, and 2.5 GPa and end at 0.5 GPa. Melting parameters as in Fig. 2. (For interpretation of color mentioned in this figure the reader is referred to the web version of the article.)

Table 1
Whole Moon, green glass source, and model magma compositions

	TWM	LPUM	GGSa	GGSp	FF40[a]	FF30[b]	Ap15G	Ap14 GrB
SiO_2	44.4	46.1	44.2	52.1	44.2	44.23	44.1	44.8
TiO_2	0.31	0.17	0.08	0.19	0.57	0.73	0.37	0.45
Al_2O_3	6.14	3.93	1.21	2.47	6.30	7.49	7.81	7.14
Cr_2O_3	0.61	0.50	0.43	1.31	0.60	0.89	0.33	0.54
FeO	10.9	7.62	16.2	12.1	22.6	21.4	21.0	19.8
MgO	32.7	38.3	36.4	29.4	18.0	16.7	16.1	19.1
MnO	0.15	0.13	0.18	0.14	0.28	0.10	0.26	0.24
CaO	4.60	3.18	1.27	2.29	7.26	8.41	8.68	8.03
K_2O	0.009	0.003	0.002	0.005	0.02	0.03	0.03	0.0
Na_2O	0.09	0.05	0.03	0.13	0.22	0.13	0.28	0.06
Mg′	.842	.900	.800	.812	.586	.573	.632	.568

[a] Accumulated melt composition: fractional fusion of GGSa source, 4.0 GPa initial melting, 0.1 GPa steps, 0.008 porosity.
[b] Accumulated melt composition: fractional fusion of GGSa source, 3.0 GPa initial melting, 0.1 GPa steps, 0.008 porosity.

different pressure (4.0, 3.0, and 2.5 GPa), but all three end at 0.5 GPa. The accumulated 0.5 GPa melts for the 4.0 and 3.0 GPa tracks are listed in Table 1. All of the instantaneous melts were saturated with olivine and orthopyroxene. The total amount of melt produced in these trajectories (13.1%, 9.1%, and 7.7%, respectively) decreases with the pressure of the onset of melting. The melting rate, which ranges from 3.6 to 3.8%/GPa, is distinctly lower than the 10%/GPa value given by Hess (1992). The reason is that the magnitude of the melting rate, -d(fxt)/dT, where fxt is the mol fraction of crystals and T is temperature, decreases as the number of solid phases is reduced—meaning that larger drops in temperature are required to produce sufficient heat to melt the same mass of peridotite. In the present case, melting of GGSa involves only olivine and orthopyroxene, whereas Hess' estimate applies to peridotites that also contain clinopyroxene and a highly aluminous phase. The onset of melting also affects melt composition: for the same initial source composition, a lower onset melting pressure produces accumulated melts that are higher in Pl and Wo components. However, as the source becomes more refractory the amount of melting also decreases, and the pressure at which the accumulated melts cross the array of green glass compositions (Pg) increases. Thus even though the polybaric track of GGSa that begins at 2.5 GPa does not cross the array of green glass compositions, it is nonetheless possible to start melting at 2.5 GPa and produce an accumulated melt that crosses the array of green glass compositions by judicious lowering of the Al_2O_3 and CaO contents of the source. For the case of a source with Al_2O_3 and CaO concentrations each equal to 0.8 wt%, Pg is 1.9 GPa (not shown) and the extent of melting is only 2.6%. Since the polybaric fractional model was devised to produce accumulated melts similar to the green glasses at relatively low pressure (Longhi, 1992), melting sequences that have Pg $\geq$ 1.5 GPa do not provide a satisfactory solution. A corollary of this observation is that sources with Al_2O_3 and CaO concentrations distinctly lower than GGSa do not provide acceptable

green glass sources in polybaric fractional melting environments.

In keeping with the recent crack propagation model of Wilson and Head (2003), a series of accumulated batch melts were also calculated. The crack-propagation model posits that exsolution of gas from a deep-seated magma into a propagating crack may generate sufficient stress to produce runaway crack growth. According to their model, the crack might extend hundreds of kilometers from the interior to the surface, thus providing a conduit through which the magma might rise rapidly to the surface relatively free of crystallization or wall–rock interaction that would modify the melt composition. A tacit assumption of this model is that melt does not disperse and percolate away by porous flow as it is generated, but rather the melting source has sufficient strength to maintain several percent porosity. For the present purposes, the depth of crack initiation would be given by the multiple saturation point on the high-pressure liquidus of the composition in question. Data summarized by Elkins-Tanton et al. (2002, 2003a) indicate pressures in the range of 1.5–2.5 GPa for the green glasses. The amount of melt depends on the initial pressure of melting and the composition. In olivine-rich systems the preservation of more than a few percent of porosity seems highly unlikely because of low wetting angles indicative of an interconnected porosity network (Waff and Bulau, 1979). Therefore, I calculated polybaric batch melting sequences for several compositions with initial melting at 3.0 GPa in order to limit the melting to approximately 5%. The trace of the melts of one of these compositions with 1 wt% Al_2O_3 and 1 wt% CaO skirts the array of green glass compositions in the range of 3.0–2.3 GPa in Fig. 7. The melting rate for this track is approximately 8.8%/GPa—close to Hess (1992) estimate. Recall from Figs. 3 and 4 that 10% batch melts of primitive compositions produced aluminous tholeiitic liquids. Relatively low Al_2O_3 source regions are thus to be expected if 5% melts are not to be tholeiitic.

2.4.2. Pyroxene-rich compositions

How unique is GGSa? Melting of at least one other low-Al source is required to account for the full range of green glasses if they are primary. On the other hand, some of the green glass compositional trends are consistent with wall-rock assimilation at 0.6–2.4 GPa (Elkins-Tanton et al., 2003a), but elimination of these potentially evolved compositions, however, does not substantially change the projection of the overall array. As I will demonstrate below, The GGSa composition is consistent with mixing of early and late-stage cumulus crystals of a magma ocean with LPUM or TWM bulk composition. The ratio of olivine to pyroxene is approximately 2:1. This ratio represents a practical upper limit to the amount of olivine, because more olivine-rich compositions will be too easily depleted in Al_2O_3 during fractional fusion and melting will stop before the accumulated sum reaches the array of green glass compositions. It is, however, possible to generate a wide range of
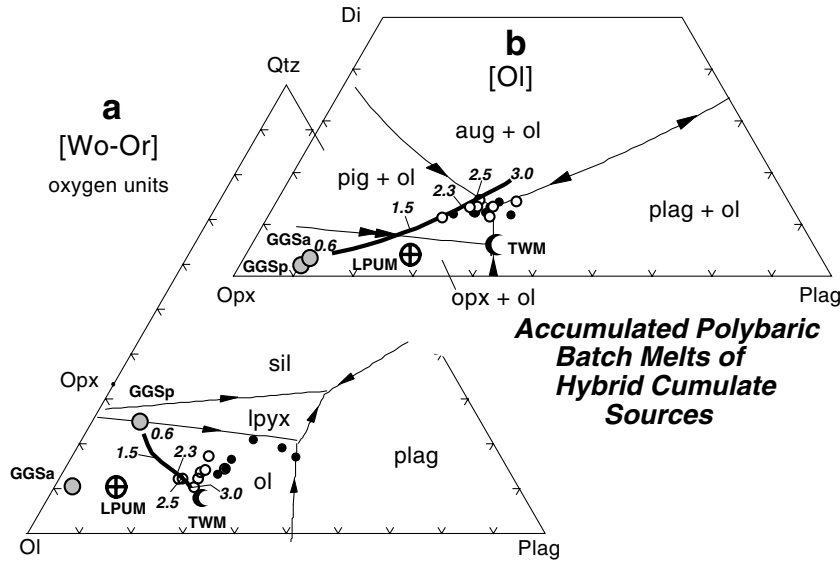
Fig. 7. Accumulated polybaric batch melts of GGSa. Projections, low-pressure phase boundaries, and symbols from Fig. 1a and b. Melting path begins at 3.0 GPa, proceeds in 0.1 GPa steps, and ends at 0.6 GPa. Melt remains in contact with the crystalline matrix from start to finish. The amount of melting in each pressure step is controlled by the temperature drop along the solidus, the adiabatic gradient, and the heat of fusion as in Fig. 2. However, in this case porosity equals the amount of melting.

source compositions that can melt to form green glass composition simply by subtracting an olivine component with $Mg' = 0.80$ from GGSa. Composition GGSp (Fig. 6 and Table 1), which is a slightly modified version of GGSa— 60% olivine, represents a practical end member for pyroxene-rich green glass source regions (the modifications are a small decrease in Al_2O_3 and a small increase in CaO in order to optimize the agreement between the array of green glasses at the low-pressure end of the trace of accumulated polybaric fractional melts. Its 4.0 GPa melting track (shown as the thin yellow curve in Fig. 6) superimposes on the GGSa accumulated melt trace that originates at 4.0 GPa. Thus, at least in terms of major elements, there is a range of possible low-Al_2O_3 source regions with variable olivine/orthopyroxene ratio.

Important implications of the calculations presented in Figs. 1–7 are that the green glass source region was significantly lower in Al_2O_3 than the Earth's depleted upper mantle (less than two-thirds and perhaps as little as one-fourth of the Earth's Al_2O_3) and that the source region extended to the depth equivalent of at least 3.0 GPa (700 km).

2.5. The significance of a low-Al source composition

2.5.1. Melt extraction

Producing low-Al_2O_3 mantle compositions simply by extracting melt typically has unacceptable consequences for other elements. The values of Mg# in LPUM and TWM (0.90 and 0.85, respectively) are already higher than that of GGSa (0.80), so extraction of any melt will leave a residue that is far too magnesian. Mg# aside, examination of GGSa in Table 1 shows sub-equal concentrations of 1.2 wt% Al_2O_3 and CaO. However, removing the 25%

batch melt of LPUM produced at 2.0 GPa (12.0 wt% Al_2O_3 and 11.8 wt% CaO) leaves an olivine–orthopyroxene residue with 1.46 wt% Al_2O_3, and 0.71 wt% CaO (the consequence of such an imbalance between Al_2O_3 and CaO is that the trace of accumulated melts will have a Wo component that is too low). Yet, if a higher degree melt is extracted from the residue, the deficit in CaO will only worsen; if less is extracted the trace of the accumulated melts will miss the array of green glasses. Similar arguments apply if the melting is fractional rather than batch. Composition GGSp presents a different sort of problem. Its Al_2O_3 content can easily be produced by modest amounts of basalt extraction, but its SiO_2 concentration (52 wt%) is problematic. Producing such a high SiO_2 by extracting melt with 44 to 45 wt% SiO_2 from a peridotitic composition like LPUM or TWM with 46 wt% SiO_2 requires more than 50% melt extraction, which, of course, undermines the entire notion of basalt extraction.

2.5.2. Mixing

Many authors have suggested hybrid mare sources are produced by overturn and mixing of the magma ocean (MO) cumulate pile (e.g., Parmentier and Hess, 1995; Elkins-Tanton et al., 2003b). Specifically, mixtures of early-crystallized magnesian olivine with later ferroan pyroxene ± plagioclase ± ilmenite. The presence or absence of plagioclase and ilmenite can be important indicators of the extent of magma ocean crystallization, and thus provide clues about the size of the ocean. Table 2 contains a mass-balance analysis of the GGSa composition in terms of calculated mineral phase compositions (Appendix A, Tables A1 and A2) taken from two magma ocean crystallization paths (Longhi, 2003). The purpose of this exercise is to determine if the GGS compositions are consistent with

Table 2
GGSa mass balance (GGSa = aOL + bOpx + cAUG + dPlag + eLPYX)

Early cumulate				Late cumulate				
		a(OL)	b(OPX)		c(AUG)	d(PLAG)	e(LPYX)	
LPUM	MO fxt[a]			MO fxt				RSSQ
fo 96	0.0	.264		0.79	−.0003	−.096	.746	48.7
fo 96	0.0	.390		0.88	−.028	−.046	.633	17.6
fo 94	0.40	.421		0.88	−.023	−.04	.599	14.1
fo 94	0.40	.592		0.94	.006	.009	.391	0.290
fo 91	0.62	.624		0.94	.012	.016	.352	0.151
fo 91	0.62	.684		0.94	.361	−.058		61.8
fo 92, en91	0.53	.610	.102	0.94	.332	−.063		60.4
fo 92, en91	0.53	.620	.006	0.94	.011	.014	.352	0.145
TWM								
fo 94	0	.529		0.90	−.0013	−.0015	.473	2.25
fo 91	0.35	.623		0.90	.012	.0156	.352	.146
fo 91	0.35	.671		0.90	.377	−.059		72.7
fo 87, en87	0.50	.637	.177	0.90	.223	−.046		26.1
fo 87, en87	0.50	.620	.111	0.90	.015	.007	.240	.044

[a] Mole fraction of the magma ocean crystallized.

the mixing hypothesis. The left hand side of the table lists early cumulate assemblages plus the mol fraction of the magma ocean (fxt) that is crystallized when the cumulate assemblage is stable at the bottom of the MO. These phases are then "mixed" with a late-stage assemblage (the fraction crystallized is given in the fifth column) consisting of augite + plagioclase ± low-Ca pyroxene by fitting the various mineral compositions to GGSa via the least-squares technique. Columns 3, 4, 6, 7, and 8 give the computed weight fractions of the phases; and the final column lists the residual sum of the squares, which in indicator of the goodness of the fit.

The results for GGSa (Table 2) show that not all combinations of cumulus minerals give good fits (RSSQ < 1.0). The LPUM liquidus olivine (fo 96) does not mix well with the late stage assemblages. Mixtures of less magnesian olivines and later stage (more ferroan) assemblages produce better fits. The results also show that mixtures lacking a late-stage low-Ca pyroxene component produced poor fits. Olivine is the dominant phase in the mixtures that give good fits, and, of these, the mixtures that have the less magnesian olivines give the better fits. The mixtures that contained early cumulus orthopyroxene provided the very best fits for both whole Moon compositions. Although 3-component mixing cannot be distinguished with the present calculations, the abundance of orthopyroxene in the better solutions is consistent with mixing of at least 3 components. One of these components may be the intermediate level assimilant hypothesized by Elkins-Tanton et al. (2003a). Finally, the mixtures that provided good fits contained only miniscule amounts (<2% each) of augite and plagioclase. Since the plagioclase component comprises roughly 50% of basaltic liquids, these calculations constrain the trapped liquid component, if there is any, to be <4%. The mixing calculations thus demonstrate that the source composition GGSa is consistent with the hypothesis of mixing of the

cumulate pile. But the mixing that produced the green glass source did not involve the most magnesian magma ocean olivines, nor did the phases that did mix come from complimentary levels of the cumulate pile (i.e., olivine that formed at 10% MO solidification did not mix with the assemblage formed at 90% solidification.).

Results of mixing calculations with the pyroxene-rich composition (GGSp) as the bulk composition (Table 3) are similar, but more restrictive than those based on the olivine-rich source. Models that combine early cumulus olivine with late-stage pyroxene and plagioclase produce residuals <1.0 only with negative proportions of plagioclase—these results imply that Al_2O_3 is too high in the bulk composition. Mixing models employing the TWM cumulate assemblages also yield negative plagioclase even when the early cumulate assemblage contains magnesian orthopyroxene. Only the LPUM mixtures containing early olivine and orthopyroxene plus late augite, low-Ca pyroxene, and plagioclase produced a low residual (0.80) and positive coefficients for all the mixing phases. The implications of the mixing calculations for the GGSp composition are thus generally similar to those for GGSa: the green glass source is probably a mixture of early cumulus olivine and orthopyroxene with later, more ferroan pyroxene and plagioclase, and/or minor trapped liquid.

What about the most magnesian magma ocean olivines? These would have been involved in the ensuing overturn of the cumulate pile (Parmentier and Hess, 1995), but not in the formation of the green glass source. Perhaps, they formed mono-mineralic layers too refractory to melt. Or, perhaps, they mixed to form the source of another phase of lunar magmatism—the magnesian suite.

2.5.3. Thermal constraints

The fact that neither batch nor polybaric melting of bulk lunar compositions can produce the picritic green glasses or mare basalts has several implications for lunar differentia-

Table 3
GGSp mass balance (GGSp = aOL + bOpx + cAUG + dPlag + eLPYX)

Early cumulate		a(OL)	b(OPX)	Late cumulate		c(AUG)	d(PLAG)	e(LPYX)	
LPUM	MO fxt				MO fxt				RSSQ
fo 96	0.0	.048			0.79	.12	−.054	.883	0.81
fo 96	0.0	.254			0.88	.118	.028	.640	9.90
fo 94	0.40	.053			0.79	.12	−.052	.876	0.71
fo 94	0.40	.267			0.88	.12	.031	.625	11.6
fo 91	0.62	.516			0.94	.18	.18	.29	54.8
fo 92, en91	0.53	.110	.637		0.94	.274	−.034		28.3
fo 92, en91	0.53	.117	.571		0.94	.057	.020	.238	0.80
TWM									
fo 94	0	.417			0.90	.154	.075	.438	34.4
fo 91	0.35	.500			0.90	.202	.094	.291	51.2
fo 91	0.35	.540			0.90	.504	.032		100.9
fo 85, en87	0.50	.104	.733		0.90	.217	−.053		11.0
fo 85, en87	0.50	.095	.692		0.90	.086	−.020	.152	.41

tion. The simplest are that: (a) the primitive isotopic and trace element patterns identified in the green glasses (e.g., Delano, 1986; Neal, 2001) are not intrinsic, but result from some sort of hybridization or assimilation; (b) the post-magma ocean deep melting of undifferentiated Moon envisioned by Kirk and Stevenson (1989) could not have produced the mare volcanics, at least not directly.

The most significant implications relate to the scale and extent of the primordial differentiation. To the extent that the model is accurate, the results imply that the differentiation event must have been sufficiently fluid to deliver differentiated material to depths of 700–1000 km. Conceivably, this transport could have been accomplished by crystallization of a magma ocean of modest depth (400–500 km) followed either by plumes of dense Fe-rich pyroxene ± ilmenite that penetrated the deep interior or by large scale overturn that placed the initially unmelted portion of the Moon above part or all of the crystallized magma ocean. Indeed, the presence of primitive components in some of the volcanic glasses (Delano, 1986) suggests that some undifferentiated isotopic components survived at least until the time of mare volcanism. However, the *P–T* path of the depleting green glass source implies that only modest amounts of undifferentiated Moon could have been present during mare volcanism (only about 20% of the Moon's volume lies below 700 km, for example).

Fig. 8 shows the pressure–temperature fractional melting paths of the GGSa and GGSp source compositions that produced the compositional trends in Fig. 6. Also plotted are the calculated solidi (2% batch melts) of GGSa and GGSp, as well as bulk Moon compositions TWM and LPUM. The plots show that the GGSa and GGSp solidus temperature are ⩾ the solidus temperatures of undifferentiated material at pressures ⩽4.0 GPa and that the fractional fusion paths of GGSa and GGSp lie at much higher temperatures than the bulk Moon solidus temperatures at pressures ⩽2.5 GPa. The reason for the more refractory nature
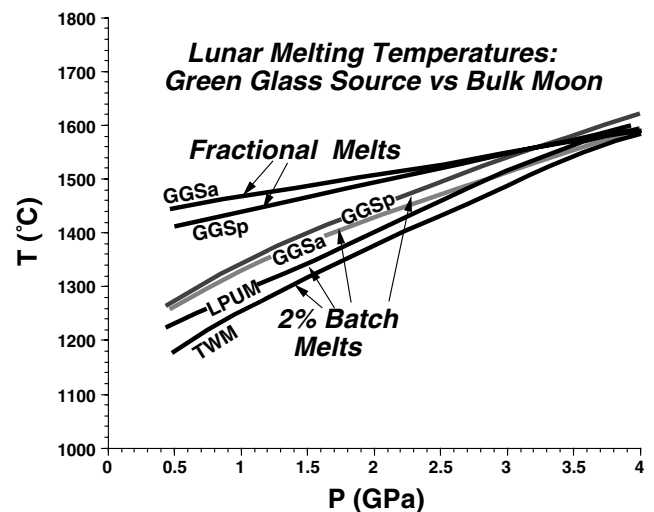

Fig. 8. Pressure–temperature track of polybaric fractional melting of GGSa and GGSp from Fig. 6 compared with solidus tracks (2% melts) of GGSa, GGSp, TWM and LPUM. Note that at pressures close to the onset of fractional melting, the GGS fractional melting paths and the GGS traces of the batch solidus cross over because the fractional melting process typically involves only ∼1% melting, which occurs at a lower temperature than a 2% melt of the same composition.

is simple: Al_2O_3 is the primary fluxing agent for anhydrous, low-alkali planetary melting. The GGS compositions not only contain sufficiently less Al_2O_3 than the whole Moon compositions to overcome the higher Mg′ values of LPUM and TWM, but the fractional melting process also progressively depletes the sources in Al_2O_3, producing more refractory *P–T* paths than the bulk solidii of the GGS compositions.

Clearly, the picritic glass magmas, generated by polybaric fractional fusion would have extensively melted and partially assimilated any primitive material with which they came into contact in the outer 400–500 km of the Moon. Equally important, however, is the observation that any primitive material in the outer 1000 km of

the Moon would have melted at lower temperature than the green glass source. Such melts would have been lunar tholeiites or even alkali-basalts in which augite was the dominant pyroxene. To the best of our knowledge, such rocks do not exist. Thus, it is not likely that any significant fraction of undifferentiated lunar material was present above ∼1000 km at the time of the green glass magmatism and, therefore, 700–1000 km is a reasonable range for the depth of the primordial differentiation. It is, of course, possible that early lunar differentiation was not entirely accomplished by a magma ocean, but also involved a stage that melted primitive portions of the Moon, not directly affected by the magma ocean, before the mare basalt era.

These inferences of depth of early melting based on green glass petrogenesis are at apparent odds with models of tectonic evolution based on initial temperature distribution. Solomon and Chaiken (1976) and Solomon (1977) showed that a planet which started out completely molten would inevitably shrink leading to large scale compression features (thrust faults) near the surface, The absence of either large scale compressional or tensional features in the Moon's crust implied a nearly constant radius through time, which could be explained by an initially hot exterior (a magma ocean) whose thermal contraction was balanced by radioactive heating and expansion of an initially cold interior. Thermal modeling by Solomon and Chaiken (1976) and Solomon (1977) yielded depths of only 200–300 km for early lunar melting. Kirk and Stevenson (1989) repeated the calculations. They found that, if they allowed for heating and melting of the primitive portion of the Moon below the magma ocean, the volume increase produced by partial melting through time could offset the contraction produced by solidification of a 600 km deep magma ocean. However, the production of this magma coincides with the eruption of the mare basalts. So unless the Moon supported two coeval, but distinct melting systems throughout its history, it is reasonable to equate the melting predicted by Kirk and Stevenson (1989) with mare basalt magmatism. But, as demonstrated above, the mare basalts could not have formed from melting the undifferentiated lunar interior. Moreover, there is no evidence of melts of primitive lunar material ever erupting as lavas. So some other means of balancing exterior contraction with interior expansion of undifferentiated material must have been at work if the models are to be reconciled. The differentiation model of Hess and Parmentier (1995) may provide a solution. They argued that overturn of the cumulate pile produced by a totally molten Moon would have brought dense late-stage cumulates and some trapped liquid, rich in heat-producing incompatible elements, into the deep interior. Radioactive decay of the isotopes of K, Th, and U in small amounts of highly enriched material in a background of mixed cumulates may have provided the heat for melting that Kirk and Stevenson (1989) attributed to chondritic levels of these elements in primitive materials.

2.6. Was there an ocean?

A final consideration is the composition of the green glass source itself. Fig. 1 illustrates the bulk compositions TWM, LPUM, GGSa, and GGSp. The first three compositions are olivine-rich and the wide spacing of their symbols reflects their different Al_2O_3 concentrations, 6, 4, and 1.2 wt%, respectively. Estimates of the difference in Al_2O_3 between primitive and depleted upper mantle on the Earth are on the order of 0.1 wt% (Kinzler and Grove, 1992b). This difference is smaller than the size of the symbols. If the Moon has a bulk composition similar to that of the earth's upper mantle, then differentiation by extraction of basalt would imply that roughly twice the mass of the green glass source had been extracted by basalt. Such material is not in evidence on the surface, and if buried would have required a remarkably cryptic history, inasmuch as any basalt would be much less refractory than either GGSa, GGSp, or undifferentiated Moon.

It is possible to constrain the depth of the green glass source further by reconsidering the phase equilibria constraints discussed above. For example, the pressures of multiple saturation on the liquidus of the picritic green glasses provide a crude estimate of the minimum depth of the mare basalt source region and, hence, the depth of early differentiation. Elkins-Tanton et al. (2002, 2003a), who summarized the latest experimental data, show values of multiple saturation pressure from 1.3 to 2.5 GPa, which correspond to depths of 260–600 km. If decompression provided most of the heat for mantle melting on the Moon, as it does on the Earth, then pressures of multiple saturation represent average depths of fractional melting (Klein and Langmuir, 1987). If one knew the total amount of melting and the melting rate as a function of pressure, it would be a relatively simple matter to calculate the initial depth of melting. The former parameter is not known, but 4.0 GPa is a reasonable upper limit in order to allow for a small lunar core and to accommodate the rapid drop-off in buoyant forces as the acceleration of gravity goes to zero at the center of the Moon (4.7 GPa). Models of green glass petrogenesis by polybaric fractional melting, which were revised above, constrain the green glass source region to lie at depths from about 700 to ⩾1000 km and contain ∼1.2 to 2.4 wt% Al_2O_3. Even polybaric batch melting followed by rapid ascent in propagating cracks—the Wilson and Head (2003) model—requires a few tenths of a GPa in excess of 2.5 GPa in order to generate a few percent of melt. These calculations thus favor a relatively deep magma ocean (⩾700 km deep), not only to produce the observed compositions of the mare volcanics, but also to avoid having a thick mantle sequence of undifferentiated bulk Moon that would have melted readily to form tholeiitic magmas that so far have not been observed.

Although the GGS compositions were developed to fit the green glasses, they are nonetheless consistent with mixing of early and late stage components of a magma ocean. These various lines of evidence thus support not only a

magma ocean, but also one that involved approximately half of the Moon's radius.

3. Mass balance constraints on bulk lunar composition

The concept of a magma ocean began with the recognition of an anorthositic crust, so it is useful to examine some mass balance constraints involving the crust. Fig. 9 illustrates the results of some simple calculations that determine the amount of Al_2O_3 residual to the formation of crusts of different thickness and composition for the two whole-Moon compositions discussed above (TWM and LPUM) and an approximate chondritic composition (C) with 3 wt% Al_2O_3. TWM and LPUM are listed in Table 1. Two cases are calculated for each whole-Moon composition, total melting (solid curves, MO = WM) and initial melting to 500 km (dashed curves, MO = 500). Following the gravity modeling of Haines and Metzger (1980), Taylor (1982) adopted 2.93 g/cm^3 and 73.4 km for the average density and thickness of the lunar highlands crust. He also derived 26 wt% Al_2O_3 as the average crustal composition. The erupted mare basalts make up a relatively small fraction of the crust, but Head and Wilson (1992) have argued that there is as much as a 50:1 ratio for intrusive to extrusive mare basalt. This ratio amounts to approximately 20% of the crust (Head and Wilson, 1992), If we take the average Al_2O_3 concentration of mare basalts to be 10 wt%, then removing the mare basalt component from the crust increases the crustal Al_2O_3 to 30 wt% and decreases the average thick-

ness to ~58 km. These values are likely to be extremes because most of the intrusive mare magmas are likely to be situated beneath maria not modeled by Haines and Metzger (1980). Employing the compositions of feldspathic lunar meteorites as random samples, Korotev et al. (2003) derived a value of 28.5 wt% Al_2O_3 for the upper crust to a depth that was well mixed by basin-forming impacts; they also noted that a more mafic lower crust was likely to be only slightly less aluminous (approximately 27 wt%). The actual Al_2O_3 concentration of the pre-mare basalt lunar crust probably thus lies within the patterned area bounded by 26 and 30 wt% Al_2O_3.

Fig. 9 shows that the chondritic (C) composition cannot satisfy the Al_2O_3 requirement of the green glass source region unless the entire Moon was initially molten, the extraction of Al_2O_3 was nearly perfect, and the average mantle was even lower in Al_2O_3 than GGSa. The TWM and LPUM compositions both contain sufficient Al_2O_3 for total melts of the Moon, but Al_2O_3 in LPUM falls short of what is needed for the green glass source regions formed from a MO < 500 km deep. Conversely, TWM contains too much Al_2O_3 for magma oceans >500 km deep. It is possible to relax the constraints on mantles that are too low in Al_2O_3 by supposing the existence of layers with very low Al_2O_3 to balance of layers with Al_2O_3 in the range of GGSa to GGSp. These very low-Al_2O_3 layers would logically be too refractory to melt and, therefore, would leave no volcanic trace. On the other hand, the constraints on mantles with Al_2O_3 concentrations that are too high cannot be relaxed because the compliment to layers with GGSa–GGSp composition would be layers with relatively high Al_2O_3, i.e., $\geqslant 4$ wt%. Such layers would be expected to melt readily and form tholeiitic magmas, which are not observed. Therefore, in terms of mass balance the TWM composition is consistent only with a relatively shallow magma ocean (<500 km). However, the constraints imposed by the petrogenesis of the green glasses require a much deeper magma ocean.

4. Other means of constraining lunar structure and bulk composition

4.1. Heat flow

Inversions of heat flow data permit estimates the bulk planetary concentrations of the refractory heat-producing elements, which in turn give the bulk concentrations of the other refractory elements (Al, Ca, Ti, and Mg), if chondritic proportions are assumed. Heat flow measurements taken at the Apollo 15 and 17 sites (2.1 and 1.6 mW/cm^2, respectively—Langseth et al., 1976; Keihm and Langseth, 1977) are consistent with 33–46 ppb of U if applied to the entire Moon. Taylor (1982) inferred from these measurements that the Moon was enriched in refractory elements—hence the high bulk Al_2O_3 concentration in TWM. Warren and Rassmusen (1987) criticized the inver-
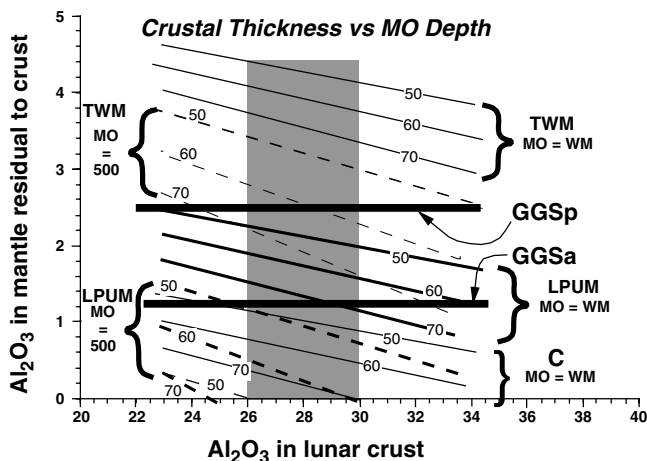

Fig. 9. Al_2O_3-mass-balance in the Moon. Al_2O_3 residual to the formation of the crust is constrained by the thickness, density, and composition of the crust. Solid lines contour crustal thickness in kilometers for an initially totally molten Moon; dashed lines contour crustal thickness for 500 km deep magma oceans (MO). Light lines are for the TWM composition (high Al_2O_3) and for the chondritic composition (C) at low Al_2O_3. Heavy contours are for the intermediate LPUM composition. Vertical shaded band sets approximate limit on crustal Al_2O_3: left margin represents Taylor (1982) average of the present crust (74 km thick); the right hand margin represents the crust prior to the mare basalts, whose hypabyssal equivalents may now comprise 20% of the crust (Head and Wilson, 1992).

sion of heat flow data, noting that the two mare sites where the measurements were taken probably were underlain by anomalously conductive crust. In light of the Clementine (Chevrel et al., 2002) and Prospector (Elphic et al., 2000; Lawrence et al., 2000) data showing the enrichment of Th (and thus presumably U) in the PKT terrane (Jolliff et al., 2000), it is clear that heat flow in this region, which includes the sites where the measurements were made, is expected to be higher than average surface values. Thus the inverted bulk Moon Th and U concentrations are likely to be too high and, likewise, the concentrations of the other refractory elements estimated by Taylor (1982) are likely to be too high, as well.

4.2. Seismology

Travel times of seismic waves can also be inverted to yield velocities, mineralogies, and densities of the media through which they travel. All of the models show an increase in density with depth. However, distinguishing mineralogical differences let alone compositional differences is not possible without some chemical model. For example, Kuskov et al. (2002) consider only primitive source regions such as chondrites and various pyrolite models. Other recent seismic models (Lognonne et al., 2003; Khan et al., 2006) are consistent with the Taylor (1982) composition. Lognonne et al. (2003), for example, developed a lunar chemical model to match their inverted velocity profile that included 28% tholeiitic crust and 10% eclogite from the Earth's mantle and 53% enstatite chondrite (from the giant impactor). Such a composition would contain little or no olivine, making generation of the mare basalts problematic; such a composition would also make the formation of tholeiitic basalts inevitable.

Khan et al. (2006) concluded that the most probable solutions to the seismic data yielded a pyroxenitic (>90% orthopyroxene and clinopyroxene) upper mantle and a lower lunar mantle that consists primarily of olivine (60) and garnet (40), although there is another family of solutions with less garnet and more pyroxene. These phase proportions should be compared not with the GGS compositions themselves, but with their residual phase proportions, which are: 70% olivine, 30% orthopyroxene for GGSa and 8% olivine, 92% orthopyroxene for GGSp. The agreement between residual GGSp and the upper mantle model is quite close considering the different approaches. Although no garnet or other aluminous phase was observed on the calculated solidii of the GGS compositions at any pressure, it is nonetheless possible that some might form at lower ambient temperatures as garnet became a more stable site for Al relative to pyroxene. However, even if all of the Al_2O_3 in the GGS compositions were to go into garnet, there could still be no more than 5–6% garnet by weight in a GGSa source and 10–12% in a GGSp source. In GGS residues the maximum amounts of garnet would be 1.5% and 6%, respectively. A more reasonable parti-

tioning that left some Al_2O_3 in the pyroxene would permit no more than 1–3% garnet in the residues. Although such low fractions of garnet are not the most probable solutions in the Khan et al. (2006) analysis, these low fractions of garnet are nonetheless within the finite probability envelopes. Thus there appears to be some hope that physical and chemical models may one day accommodate one another.

5. Conclusions

There are important differences between lunar and terrestrial basalts that reflect more on the different styles of planetary differentiation than on different bulk compositions. The compositions of the most common terrestrial basalts reflect source compositions in which the major elements are only weakly fractionated with respect to their chondritic precursors. The compositions of the mare volcanics, particularly the green glasses, constrain the mare basalt source region to be low in Al_2O_3—from about 1.2% for olivine-rich sources to 2.4 wt% for pyroxene-rich sources. Such compositions require formation by accumulation in a magma ocean; they cannot be formed basalt extraction, because depletions of CaO would be too severe in olivine-rich sources; and enrichments in SiO_2 would be too meager in pyroxene-rich sources. The deep, low-Al_2O_3 sources of the mare volcanics, required by polybaric fractional fusion models, produce pressure–temperature tracks that are also more refractory than any of the undifferentiated bulk compositions. Thus, the presence of low-Al_2O_3 magmas and the absence of tholeiites during mare volcanism implies not only low-Al sources, but the absence of undifferentiated material down to the depths where melting of the green glass sources were initiated (700–1000 km). Mass balance calculations based on estimates of crustal thickness and composition show the refractory-rich bulk Moon composition proposed by Taylor (1982) with 6 wt% Al_2O_3 would have had a mantle that was far too rich in Al_2O_3 to satisfy the constraints of the green glass source regions. Estimates of the lunar bulk composition, similar to the Earth's upper mantle, with approximately 4 wt% Al_2O_3, do, however, satisfy the constraints.

Associate Editor: Clive R. Neal

Appendix A

A.1. Calculation of melting and crystallization

The strategy and procedures by which the calculations of high-pressure melting and crystallization are carried out have already been described in considerable detail (Longhi, 2002 and Longhi, 2003). However, a major recalibration of pressure in $BaCO_3$ piston–cylinder assemblies (Longhi, 2005) has necessitated updates of the various algorithms used to determine phase stability, temperature, and pressure. Accordingly, a new illustration of the agreement between the reported and calculated locus of liquids saturated with olivine and orthopyroxene ± clinopyroxene ± garnet ± spinel is shown in Figure A1. For each of the *ol* +*opx*-saturated liquids a section of the *ol* + *opx* liquidus boundary curve was calculated from the pressure, Wo content, Mg′, and normative feldspar composition of the liquid. Ideally, each point should have a section of the *ol* + *opx* liquidus boundary passing through it. To avoid clutter, the tested compositions are separated into two groups: (a) data generated at LDEO; and (b) data taken from the literature.

A.2. Inputs to GGS mineral component calculations

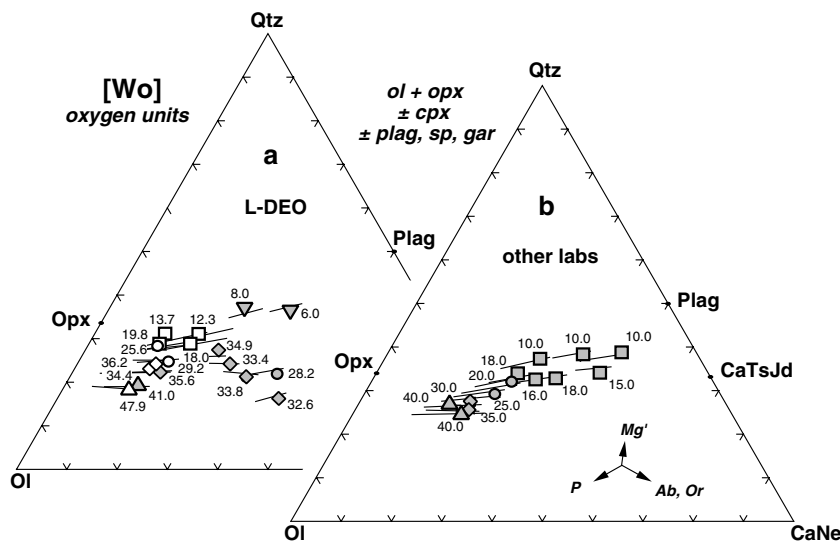The mineral compositions used as inputs to the GGS mixing calculations (Tables 2 and 3) are listed in Tables

Fig. A1. Performance of the current crystallization/melting model for the *ol* + *opx* liquidus boundary curve. Compositions are projections from Wollastonite ($CaSiO_3$) component {Wo} onto the olivine (Ol)–calcium aluminate-nepheline (CaNe)–quartz (Qtz) plane. Open symbols indicate only coexisting *ol* + *opx* (or *pig*).; solid symbols indicate coexisting *gar*, *sp*, or *plag* as well. Short segments of the *ol* + *opx* liquidus boundary curve are calculated for each liquid given the pressure, Mg′, and normative feldspar composition after Longhi (1991). Numbers indicate pressure in GPa × 10. (a) Lamont-Doherty calibration set; all pressures recalculated according to the empirical correction derived by Longhi (2005). (b) Calibration set from other labs. Reference for all data sets given by Longhi (2003).

Table A1
Lunar primitive upper mantle (LPUM) magma ocean crystallization products (wt% oxides) after Longhi (2003)

	Early cumulates					Late cumulates			Late cumulates		
fxt[a]	0.0	0.40	0.62	0.53	0.53	0.88	0.88	0.88	0.96	0.96	0.96
GPa[b]	4.0	1.71	0.94	1.38	1.38	0.31	0.31	0.31	0.08	0.08	0.08
	ol	ol	ol	ol	opx	opx	plag	aug	opx	plag	aug
	fo 96	fo 94	fo 91	fo 92	en 91	en 21	an98	wo42	wo2.3	an97	wo44
SiO_2	41.8	41.4	41.0	40.2	55.0	52.4	44.3	50.4	49.4	44.6	49.1
TiO_2	0.0	0.0	0.0	0.0	0.08	0.21	0.0	0.60	0.35	0.0	1.08
Al_2O_3	0.04	0.05	0.01	0.10	3.86	2.85	35.2	3.70	1.88	35.1	2.53
Cr_2O_3	0.46	0.61	0.49	0.81	0.83	0.38	0.0	0.99	0.18	0.0	0.56
FeO	3.87	5.64	7.67	11.6	6.81	19.1	0.37	10.1	32.4	0.45	16.8
MgO	53.7	52.1	50.4	47.0	32.2	23.6	0.23	13.8	14.0	0.15	9.09
MnO	0.08	0.09	0.12	0.14	0.10	0.38	0.0	0.20	0.67	0.0	0.35
CaO	0.12	0.17	0.24	0.32	1.10	1.04	19.7	20.7	1.06	19.5	20.5
Na_2O	0.0	0.0	0.0	0.0	0.0	0.0	0.24	0.03	0.01	0.37	0.07

[a] Mole fraction of magma ocean crystallized.
[b] Pressure at bottom of the magma ocean.

Table A2
Taylor Whole Moon (TWM) magma ocean crystallization products (wt% oxides) after Longhi (2003)

	Early cumulates				Late cumulates		
fxt	0.0	0.34	0.50	0.50	0.90	0.90	0.90
GPa	3.0	2.5	1.47	1.47	0.20	0.20	0.20
	ol	ol	ol	opx	opx	plag	aug
	fo 94	fo 91	fo 88	en 87	en53	an95	wo43
SiO_2	41.4	41.0	40.2	55.0	50.5	44.9	49.4
TiO_2	0.0	0.0	0.0	0.08	0.35	0.0	0.96
Al_2O_3	0.05	0.01	0.10	3.86	2.67	34.8	3.52
Cr_2O_3	0.61	0.49	0.81	0.83	0.30	0.0	0.80
FeO	5.64	7.67	11.6	6.81	26.4	0.45	13.85
MgO	52.1	50.4	47.0	32.2	18.2	0.15	11.1
MnO	0.09	0.12	0.14	0.10	0.45	0.0	0.24
CaO	0.17	0.24	0.32	1.10	1.16	19.2	20.10
Na_2O	0.0	0.0	0.0	0.0	0.01	0.55	0.07

A1 and A2. These compositions were calculated by Longhi (2003) for fractional crystallization of LPUM and TWM magma oceans with initial basal pressures of 3.0 GPa. The extent of MO crystallization is expressed as the mole fraction. Phase compositions are listed as weight per cent oxides.

References

Basaltic Volcanism Study Project, 1981. *Basaltic Volcanism on the Terrestrial Planets*. Pergamon, New York, 1286 pp.

Chevrel, S.D., Pinet, P.C., Daydou, Y., Maurice, S., Lawrence, D.J., Feldman, W.C., Lucey, P.G., 2002. Integration of the Clementine UV–vis spectral reflectance data and the lunar prospector gamma-ray spectrometer data: a global-scale multielement analysis of the lunar surface using iron, titanium, and thorium abundances. *J. Geophys. Res. Planets* **107** (E12), 15/1–15/14.

Delano, J.W., 1986. Pristine lunar glasses: criteria, data, and implications. In: *Proceedings of the 16th Lunar Planetary Science Conference, J. Geophys. Res.,* **91**, pp. D201–D213.

Elkins-Tanton, L.T., Van Orman, J.A., Hager, B.H., Bradford, H., Grove, T.L., 2002. Re-examination of the lunar magma ocean cumulate overturn hypothesis: melting or mixing is required. *Earth Planet. Sci. Lett.* **196** (3–4), 239–249.

Elkins-Tanton, L.T., Chatterjee, N., Grove, T.L., 2003a. Experimental and petrological constraints on lunar differentiation from the Apollo 15 green picritic glasses. *Meteorit. Planet. Sci.* **38** (4), 515–527.

Elkins-Tanton, L.T., Parmentier, E.M., Hess, P.C., 2003b. Magma ocean fractional crystallization and cumulate overturn in terrestrial planets: implications for Mars. *Meteorit. Planet. Sci.* **38** (12), 1753–1771.

Elphic, R.C., Lawrence, D.J., Feldman, W.C., Barraclough, B.L., Maurice, S., Binder, A.B., Lucey, P.G., 2000. Lunar rare earth distributions and ramifications for FeO and TiO2: lunar prospector neutron spectrometer observations. *J. Geophys. Res.* **105**, 20,333–20,345.

Green, D.H., Ware, N.G., Hibberson, W.O., Major, A., 1971a. Experimental petrology of Apollo 12 basalts: Part 1, sample 12009. *Earth Planet. Sci. Lett.* **13**, 85–96.

Green, D.H., Ringwood, A.E., Ware, N.G., Hibberson, W.O., Major, A., Kiss, E., 1971b. Experimental petrology and petrogenesis of Apollo 12 basalts. In: *Proceedings of the 2nd Lunar Science Conference*, pp. 601—615.

Haines, E.L., Metzger, A.E., 1980. Lunar highland crustal models based on iron concentrations: isostasy and center-of-mass displacements. In: *Proceedings of the 11th Lunar Science Conference*, pp. 698–718.

Hart, S.R., Zindler, A., 1986. In search of a bulk-Earth composition. *Chem. Geol.* **57**, 247–267.

Head, J.W., Wilson, L., 1992. Lunar mare volcanism: stratigraphy, eruption conditions, and the evolution of secondary crusts. *Geochim. Cosmochim. Acta* **56**, 2155–2175.

Hess, P.C., 1992. Phase equilibrium constraints on the origin of ocean floor basalts. In: *Mantle Flow and Melt Generation at Mid-Ocean RidgesGeophysical Monograph*, vol. 71. American Geophysical Union, pp. 67–102.

Hess, P.C., Parmentier, E.M., 1995. A model for the thermal and chemical evolution of the Moon's interior: implications for the onset of mare volcanism. *Earth Planet. Sci. Lett.* **134**, 501–514.

Hirschmann, M.M., Ghiorso, M.S., Wasylenki, L.E., Asimow, P.D., Stolper, E.M., 1998. Calculation of peridotite partial melting from thermodynamic models of minerals and melts: I. Review of methods and comparison with experiments. *J. Petrol.* **39**, 1091–1115.

Jolliff, B.L., Gillis, J.J., Haskin, L.A., Korotev, R.L., Wieczorek, M.A., 2000. Major lunar crustal terranes: surface expressions and crust-mantle origins. *J. Geophys. Res.* **105**, 4197–4216.

Keihm, S.J., Langseth, M.G., 1977. Lunar thermal regime to 300 km. In: *Proceedings of the 8th Lunar Science Conference*, pp. 499–514.

Khan, A., Maclennan, J., Taylor, S.R., Connolly, J.A.D., 2006. Are the Earth and Moon compositionally alike? Inferences on lunar composition and implications for lunar origin and evolution from geophysical modeling. *J. Geophys. Res. Planets* **111** (E5), E05005–E05006.

Kinzler, R.J., Grove, T.L., 1992a. Primary magmas of mid-ocean ridge basalts 1. Experiments and methods. *J. Geophys. Res.* **97**, 6907–6926.

Kinzler, R.J., Grove, T.L., 1992b. Primary magmas of mid-ocean ridge basalts 2. Applications. *J. Geophys. Res.* **97**, 6907–6926.

Kirk, R.L., Stevenson, D.J., 1989. The competition between thermal contraction and differentiation in the stress history of the Moon. *J. Geophys. Res.* **94**, 12,133–12,144.

Klein, E.M., Langmuir, C.H., 1987. Global correlation of ocean ridge basalt chemistry with axial depth and crustal thickness. *J. Geophys. Res.* **92**, 8089–8115.

Korotev, R.L., Jolliff, B.L., Zeigler, R.A., Gillis, J.J., Haskin, L.A., 2003. Feldspathic lunar meteorites and their implications for compositional remote sensing of the lunar surface and the composition of the lunar crust. *Geochim. Cosmochim. Acta* **67** (24), 4895–4923.

Kuskov, O.L., Kronrod, V.A., Hood, L.L., 2002. Geochemical constraints on the seismic properties of the lunar mantle. *Phys. Earth Planet. Inter.* **134** (3–4), 175.

Langseth, M.G., Keihm, S.J., Peters, K., 1976. Revised lunar heat flow values. In: *Proceedings of the 7th Lunar Science Conference*, pp. 3141–3171.

Lawrence, D.J., Feldman, W.C., Barraclough, B.L., Binder, A.B., Elphic, R.C., Maurice, S., Miller, M.C., Prettyman, T.H., 2000. Global elemental maps of the Moon. *Science* **281**, 1484–1489.

Lognonne, P., Gagnepain-Beyneix, J., Chenet, H., 2003. A new seismic model of the Moon: implications for structure, thermal evolution and formation of the Moon. *Earth Planet. Sci. Lett.* **211** (1–2), 27–44.

Longhi, J., 1991. Comparative liquidus equilibria of hypersthene-normative basalts at low pressure. *Am. Miner.* **76**, 785–800.

Longhi, J., 1992. Origin of green glass magmas by polybaric fractional fusion. *Proc. Lunar Planet Sci.* **22**, 343–353.

Longhi, 2002. Some phase equilibrium systematics of lherzolite melting: I. *Geochem. Geophys. Geosyst.*, 10.1029/2001GC000204.

Longhi, J., 2003. A new view of lunar ferroan anorthosites: post magma ocean petrogenesis. *J. Geophys. Res.* **108**, 10 .1029/202JE001941.

Longhi, J., 2005. Temporal stability and pressure calibration of barium carbonate and talc/pyrex pressure media in a piston–cylinder apparatus. *Am. Miner.* **90**, 206–218.

McKenzie, D., 1984. The generation and compaction of partially molten rock. *J. Petrol.* **25**, 713–765.

Melson, W.G., Vallier, T.L., Wright, T.L., Byerly, G., Nelen, J., 1976. Chemical diversity of abyssal volcanic glass erupted along Pacific, Atlantic, and Indian Ocean sea-floor spreading centers. In: *The Geophysics of the Ocean Basin and Its Margins*. America Geophysics Union, Washington, DC, pp. 351–367.

Neal, C.R., 2001. Interior of the Moon: the presence of garnet in the primitve deep lunar mantle. *J. Geophys. Res.* **106** (27), 865–886.

Parmentier, E.M., Hess, P.C., 1995. A model for the thermal and chemical evolution of the Moon's interior; implications for the onset of mare volcanism. *Earth Planet. Sci. Lett.* **134**, 501–514.

Philpotts, J.A., Schnetzler, C.C., Nava, D.F., Bottino, M.L., Fullagar, P.D., Thomas, H.H., Schumann, S., Kouns, C.W., 1972. Apollo 14: some geochemical aspects. In: *Proceedings of Third Lunar Planetary Science Conference*. The MIT Press, pp. 1293–1305.

Salters, V., Longhi, J., Bizimus, M., 2002. Near mantle solidus trace element partitioning at pressures up to 3.4 GPa. *Geochem. Geophys. Geosyst.* **3**. doi:10.1029/2001/GC000148.

Solomon, S.C., 1977. The relationship between crustal tectonics and internal evolution in the Moon and Mercury. *Phys. Earth Planet. Inter.* **15**, 135–145.

Solomon, S.C., Chaiken, J., 1976. Thermal expansion and thermal stress in the Moon and terrestrial planets: clues to early thermal history. In: *Proceedings of the 7th Lunar Science Conference*, pp. 3229–3243.

Solomon, S.C., Töksoz, M.N., 1973. Internal constitution and evolution of the Moon. *Phys. Earth Planet. Inter.* **7**, 15–38.

Taylor, S.R., 1982. *Planetary Science: A Lunar Perspective*. The Lunar & Planetary Inst., Houston.

Taylor, S.R., Jakés, P., 1974. The geochemical evolution of the moon. In: *Proceedings of the 5th Lunar Science Conference*, pp. 1287–1305.

Waff, H.S., Bulau, J.R., 1979. Equilibrium fluid distribution in an ultramafic partial melt under hydrostatic stress conditions. *J. Geophys. Res.* **84**, 6109–6114.

Warren, P.W., 1985. The magma ocean concept and lunar evolution. *Annu. Rev. Earth Planet. Sci.* **13**, 201–240.

Warren, P.W., Rassmusen, K.L., 1987. Megaregolith insulation, internal temperatures, and bulk uranium content of the Moon. *J. Geophys. Res.* **92**, 3453–3465.

Wilson, L., Head, J.W., 2003. Deep generation of magmatic gas on the Moon and implications for pyroclastic eruptions. *Geophys. Res. Lett.* **30**, 10.1029/2002GL016082.

Wood, J.A., 1975. Lunar petrogenesis in a well-stirred magma ocean. In: *Proceedings of the 6th Lunar Science Conference*, pp. 1087–1102.

Wood, J.A., Dickey Jr., J.S., Marvin, U.B., Powell, B.N., 1970. Lunar anorthosites and a geophysical model of the moon. In: *Proceedings of the Apollo II Lunar Science Conference*, pp. 965–988.